Hybrid stars and the QCD phase transition with an NJL-type model

Bing-Jun Zuo,[1,*] Yong-Feng Huang,[2,3,†] and Hong-Tao Feng[4]

[1]*Department of Physics, Nanjing University, Nanjing 210093, China*
[2]*School of Astronomy and Space Science, Nanjing University, Nanjing 210023, China*
[3]*Key Laboratory of Modern Astronomy and Astrophysics (Nanjing University), Ministry of Education, Nanjing 210023, China*
[4]*School of Physics, Southeast University, Nanjing 211189, China*

(Received 27 October 2021; accepted 21 March 2022; published 18 April 2022)

In this paper we introduce a self-consistent mean field approximation to study the QCD phase transition and the structure of hybrid stars within the framework of an NJL-type model. In our practice, a phenomenological parameter α is introduced, which reflects the weights of the "direct" channel and "exchange" channel under a finite chemical potential. The mass-radius relation is obtained by solving the Tolman-Oppenheimer-Volkoff equation using a crossover equation of state (EOS). We calculate the density distribution in a two solar-mass hybrid star to show the effects of different parameters. We also calculate the tidal Love number k_2 and the deformability (Λ). It is found that the stiffness of the EOS increases with α, which allows us to obtain a hybrid star with a maximum mass of 2.40 solar mass through our model. The observation of over 2.06 solar-mass neutron stars may indicate that the chiral transition may be a crossover on the whole T-μ plane.

DOI: 10.1103/PhysRevD.105.074011

I. INTRODUCTION

Neutron stars are the densest celestial bodies in our Universe except for black holes. Their extreme environment provides us a natural laboratory for cold and condensed matter. In recent years, the detection of gravitational waves has given us different valuable information about compact stars. During the inspiral and merger of binary stars, the tidal deformability can be measured by the LIGO and VIRGO network directly [1]. The Love number k_2 is used to measure the distortion of a neutron star. It can be calculated through the exterior solutions that are related to the tidal deformability (Λ) [2–4]. On the other hand, electromagnetic observations on the cooling rate [5], gamma-ray bursts [6], thermal x rays [7], and radio bursts [8] from neutron stars give us diverse data to study neutron stars. These astronomical observations can help us to constrain theoretical models and improve our understanding of neutron stars.

The inner structure of neutron stars is still not well known. The possibility that the neutron star is composed of a quark-matter inner core, nucleon matter outer core and crust, i.e., being a hybrid star, is widely discussed. The key to studying hybrid stars is the equation of state (EOS) of the strongly-interacting matter. For quark matter, lattice quantum chromodynamics (LQCD) is widely accepted as the *ab initio* method to deal with QCD nonperturbatively. Unfortunately, present lattice QCD calculations at finite chemical potential are plagued with the so-called sign problem [9]. Thus, to study QCD systems at finite chemical potential, it is necessary to employ some QCD effective models, such as the Nambu-Jona-Lasinio (NJL) model [10–14]. The NJL model displays important features of QCD, i.e., the dynamical chiral symmetry breaking and restoring. The chiral restoring phase transition is usually considered to happen simultaneously (or almost simultaneously) with the deconfinement phase transition [15–18]. Thus, a problem naturally arises; which type of phase transition should it be, a first-order phase transition or a crossover?

Another related issue is that in the case of zero chemical potential and finite temperature, the result of LQCD and other methods shows there is a crossover [15–18]. Thus, at zero temperature and finite chemical potential the type of phase transition determines whether there exists a critical end point (CEP) in the QCD phase diagram. Experimentally, the second stage beam energy scanning plan of the Relativistic Heavy Ion Collider (RHIC) is still to try to find the possible CEP [19–21]. Theoretically, different models give different perspectives and answers. In this paper, we will study this issue by using a self-consistent mean field approximation in the framework of the NJL model [22]. People generally predict that the hadronic matter will completely transition to quark matter when the density increases to 4–8 times the saturation density of the nucleon matter in the hadron physical pictures. [23–26],

*812380695@qq.com
†hyf@nju.edu.cn

which means that the corresponding quark chemical potential is at least larger than 430 MeV in NJL model. However, the strong interaction phase transition predicted by the standard NJL model usually occurs near 330 MeV [27–30], which indicates that there is an contradiction between the prediction of the standard NJL model and the corresponding prediction of the hadron physical pictures.

In order to overcome this contradiction, the authors of Ref. [22] proposed a mean field approximation method under the framework of the NJL model. In this method, a phenomenological parameter α is introduced to reflect the weights of the "exchange" channel and "direct" channel, because the vector interaction term generated by the "exchange" channel plays a very important role in the case of finite chemical potential. The relative results will influence the CEP and hybrid stars. α is a theoretical parameter and the finite density experiments could help to constrain α. For example, the experiments of RHIC can provide useful clues on the issue of whether the CEP exists or not, which itself can help constrain the value of α. Anyway, note that such a constraint will still be too rough to determine α exactly, since there may be other factors influencing the CEP. Thus, we need various experiments and observations, such as the astronomical observations of neutron stars, to further constrain the parameter. Another point we focus on is the uncertain region between the nucleon matter and the quark matter. The uncertainty forces us to adopt some nonphysical methods to connect the nucleon part and the quark part, such as the Gibbs construction [31], or other mathematical operations [24,32,33]. However, these methods unavoidably lead to a phase transition themselves, thus they are not self-consistent in the practice. The EOS will be studied under a crossover-type model with a self-consistent connection method in this paper.

This paper is organized as follows. In Sec. II we introduce the three-flavor NJL model and its Fierz transformation. The three-flavor QCD phase diagram is calculated and the existence of the CEP in our model is discussed. In Sec. III the thermodynamical relations will be solved to obtain the EOS for quark matter. We use the soft-hadronic Akmal-Pandharipande-Ravenhall (APR) EOS [34] and a crossover connection method to get the EOS of hybrid stars. We will show how hybrid stars are changed in this framework. Finally, we give a summary in Sec. IV.

II. MEAN FIELD APPROXIMATION AND PHASE TRANSITION

The standard $(2+1)$-flavor NJL Lagrangian contains four-fermion and six-fermion interactions written as

$$\mathscr{L} = \bar{\psi}(i\partial\!\!\!/ - m)\psi + G\sum_{a=0}^{8}[(\bar{\psi}\lambda^a\psi)^2 + (\bar{\psi}i\gamma_5\lambda^a\psi)^2] - K[\det\bar{\psi}(1+\gamma_5)\psi + \det\bar{\psi}(1-\gamma_5)\psi] + \mu\psi^\dagger\psi, \quad (1)$$

where m is the current quark mass, and G and K denote the coupling constants which will be calibrated to reproduce the physical pion meson mass, kaon meson mass, and their decay constant. The corresponding mean field approximation is

$$\mathscr{L}_1 \approx \bar{\psi}[i\partial\!\!\!/ - \gamma^0\mu - (m+\mathbf{A})]\psi, \quad (2)$$

with

$$\mathbf{A} = -4G\begin{pmatrix}\sigma_u & & \\ & \sigma_d & \\ & & \sigma_s\end{pmatrix} + 2K\begin{pmatrix}\sigma_d\sigma_s & & \\ & \sigma_u\sigma_s & \\ & & \sigma_u\sigma_d\end{pmatrix},$$

and

$$\sigma_i = \langle\bar{\psi}_i\psi_i\rangle = -\int\frac{d^4p}{(2\pi)^4}\mathrm{Tr}[s(p)_i] \qquad i = u,d,s,$$

where σ is the quark condensation, Tr denotes a trace over color and spinor indices.

As shown in Eq. (1), the standard NJL model Lagrangian contains only the interactions of scalar and pseudoscalar channels. It is insufficient to handle the interaction of vector channels, such as in the case of finite chemical potential. To get a self-consistent result in the sense of mean field approximation, the contribution of Fierz transformation Lagrangian must be taken into account [35]. The authors of Ref. [11] demonstrated that a Fierz transformation of a six-fermion interaction can be defined as an operation that leaves the interaction invariant under all possible permutations of the quark spinors ψ occurring in it; thus, the six-fermion term does not change after Fierz transformation. So in this paper we only need to consider the Fierz transformation of four-fermion term, which can be written as [11]

$$\mathscr{F}\left[\sum_{a=0}^{8}[(\bar{\psi}\lambda^a\psi)^2 + (\bar{\psi}i\gamma_5\lambda^a\psi)^2]\right] = -\frac{G}{2}\sum_{c=0}^{8}[(\bar{\psi}\gamma^\mu\lambda^c\psi)^2 - (\bar{\psi}\gamma^\mu\gamma^5\lambda^c\psi)^2]. \quad (3)$$

In this study, we only consider the scalar and vector channel contribution, this is because other terms in our modeling make no contribution at the level of the mean field approximation. The mean field approximation of the Fierz transformation of the original NJL Lagrangian is

$$\mathscr{L}_2 \approx \bar{\psi}[i\partial\!\!\!/ - \gamma^0(\mu+\boldsymbol{B}) - (m+\boldsymbol{A})]\psi. \quad (4)$$

Here $\boldsymbol{B} = -\frac{2G}{3}(n_u+n_d+n_s)\boldsymbol{I}$, where $\boldsymbol{I}$ is the identity matrix in flavor space and n denotes the quark number density. $\mathscr{L}_1$ contains only the Hartree term, while $\mathscr{L}_2$

contains only the Fock term. We can rewrite Eq. (1) by taking the linear combination of $\mathscr{L}_1$ and $\mathscr{L}_2$ [22],

$$\mathscr{L}_R = (1-\alpha)\mathscr{L}_1 + \alpha\mathscr{L}_2. \tag{5}$$

To illustrate the characteristics of this approach, let us recall the mean field approximation utilized in previous studies within the framework of the NJL model. In the original mean field approximation, the Fierz transformation is not adopted, which corresponds to the case of $\alpha = 0$ in our method [36]. But as pointed out in Refs. [35,37], this approximation is theoretically not self-consistent at the level of the mean field approximation.

As shown in Refs. [35,37], to get a self-consistent result in the sense of mean field approximation, the contribution of the Fierz transformed Lagrangian ("exchange channel") must be taken into account. Later, when the finite chemical potentials (in this situation, the vector-isoscalar channel interactions are very important) are involved, people usually put a vector-isoscalar channel interaction by hand into the original Lagrangian, so they must phenomenologically introduce a coupling parameter to reflect the strength of the explicit vector-isoscalar channel interaction [38]. This will cause a serious problem, that is, the vector-isoscalar channel interaction is introduced phenomenologically, and the Lagrangian at this time is no longer the original Lagrangian. What is more serious is that the vector-isoscalar interaction introduced by hand is not theoretically self-consistent in the framework of the mean field approximation, because the Fierz transformed Lagrangian is not considered.

At the same time, if people want to discuss the problems related to the axial-vector chemical potential (under these circumstances, the axial-vector channel interaction plays an extremely important role), then people must artificially introduce the axial-vector channel interaction. So, the introduction of a term by hand is quite arbitrary and will make the method lose its reliability [39]. In order to overcome the arbitrariness brought by the above method, the self-consistent mean field approximation method is necessary, which can release all the interaction channels hidden in the original Lagrangian by the Fierz transformation [40]. Because the Fierz transformation is an equivalent transformation, the new Lagrangian $\mathscr{L}_R = (1-\alpha)\mathscr{L} + \alpha\mathscr{L}_F$ used in this paper is equivalent to the original NJL model, which is another advantage of our method.

There are many studies that have considered the contribution of an explicit Fierz transformed term and have chosen the weight of the vector-isoscalar channel factor α as 0.5 [11,27]. However, there is no physical basis supporting that the "direct" channel and the "exchange" channel have the same weight. In principle, the value of α could be constrained or hinted from related experiments and neutron star observations. On the other hand, in the commonly used NJL model, μ_0 (when the chemical potential μ is smaller than the critical value μ_0, the quark number density becomes zero.) is very close to μ_c (the critical chemical potential of chiral restoration). It means that a vacuum phase transition occurs shortly after the baryon is excited from the vacuum, which is physically unreasonable [24,41]. This long-standing problem can be solved by adopting our self-consistent mean field approximation.

Based on the new Lagrangian of Eq. (5), the three-flavor quark gap equation is then given by

$$M_i = m_i - 4G\sigma_i + 2K\sigma_j\sigma_k, \tag{6}$$

$$\tilde{\mu}_i = \mu_i - \frac{2}{3}\alpha G'(n_u + n_d + n_s), \tag{7}$$

where $G' = \frac{G}{1-\alpha}$, and $\tilde{\mu}_i$ is the effective chemical potential and M_i is the constituent quark mass. Similarly, μ_i is the chemical potential and m_i is the quark mass. Because the NJL model is nonrenormalizable in this study we employ a three-momentum cutoff scheme to regulate the divergence. The quark condensation and number density in three-momentum cutoff scheme is given by

$$\sigma_i = -\frac{N_c M_i}{\pi^2}\int_0^\Lambda \frac{p^2}{E_{p,i}}[1 - (e^{\frac{E_{p,i}-\tilde{\mu}_i}{T}}+1)^{-1} - (e^{\frac{E_{p,i}+\tilde{\mu}_i}{T}}+1)^{-1}]dp, \tag{8}$$

$$n_i = \frac{N_c}{\pi^2}\int_0^\Lambda p^2\left[\frac{1}{e^{\frac{E_{p,i}-\tilde{\mu}_i}{T}}+1} - \frac{1}{e^{\frac{E_{p,i}+\tilde{\mu}_i}{T}}+1}\right]dp. \tag{9}$$

The parameters of NJL we adopted are shown in Table I, which are consistent with the experimental results of π, K, and η meson masses and decay constants [42].

We can use the method of finite-temperature field theory [43] to write the grand canonical potential density as

$$\Omega = \frac{-N_c T}{\pi^2}\sum_{i=u,d,s}\int p^2\left[\frac{E_{p,i}}{T} + \ln(1+e^{-\frac{E_{p,i}+\tilde{\mu}_i}{T}}) + \ln(1+e^{-\frac{E_{p,i}-\tilde{\mu}_i}{T}})\right]dp + 2G(\sigma_u+\sigma_d+\sigma_s) - \frac{\alpha G'}{3}(n_u+n_d+n_s)^2 - 4K\sigma_u\sigma_d\sigma_s + \Omega_0. \tag{10}$$

From this, the pressure $p = -\Omega$ and the energy density $\epsilon = -p + \sum_i \mu_i n_i$ can be easily obtained. In addition, the baryon number and electric charge are conserved for

TABLE I. Parameters adopted in our calculations.

m_u[MeV]	m_s[MeV]	Λ_{UV}[MeV]	$G\Lambda_{\mathrm{UV}}^2$	$K\Lambda_{\mathrm{UV}}^5$
5.5	135.7	630.1	1.781	9.29

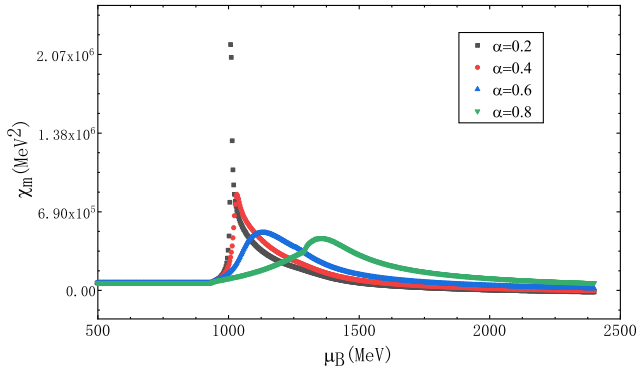

FIG. 1. The chiral susceptibility as a function of baryon chemical potential at zero temperature, for different α.

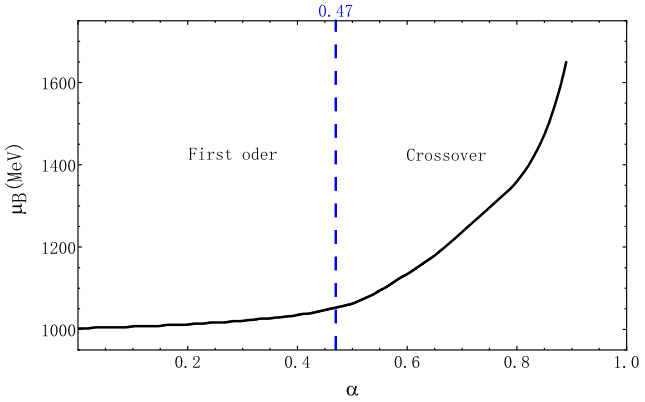

FIG. 2. The critical (pseudocritical) chemical potential as a function of α at zero temperature. When $\alpha < 0.47$, it is a first-order phase transition. But when $\alpha > 0.47$, the phase transition is a crossover.

neutron stars [44]. Therefore, we need to include the following equilibrium condition

$$\begin{cases} \frac{2}{3}n_u - \frac{1}{3}n_d - \frac{1}{3}n_s - n_e = 0, \\ \mu_e = \mu_\mu = \mu_d - \mu_u, \\ \mu_d = \mu_s. \end{cases}$$

The NJL model with zero-bare quark mass at the high-energy scale, keeps the chiral symmetry. With the decrease of energy, the quarks and antiquarks condensate together to give quarks dynamical mass, thus the chiral symmetry is broken at the low-energy scale. To illustrate this phase transition more clearly, we can use the chiral susceptibility to reveal the order of phase transition and the corresponding physical condition [45,46]. The chiral susceptibility is defined as

$$\chi_m = -\frac{\partial \sigma_u}{\partial m_u}. \tag{11}$$

We show the results of chiral susceptibility for different α in Fig. 1. It can be seen that when α is small, there is a singular point on the susceptibility curve. It corresponds to a first-order phase transition occurring at a particular critical chemical potential. On the other hand, when α is large enough ($\alpha > 0.47$), the curve becomes relatively smooth. It means that the phase transition changes to a crossover, and the chemical potential corresponding to the peak point is regarded as "pseudocritical chemical potential". Fig. 1 also shows that the critical (pseudocritical) chemical potential gradually becomes larger with the increase of the parameter α. We can see this more clearly in Fig. 2. The above results indicate that our quark model can be used to describe different kinds of phase transitions. By evaluating the parameter α properly, it can present a good approximation for various hadron models.

Similarly, using the chiral susceptibility we can plot the QCD phase diagram for different α. The result is shown in Fig. 3. In particular, we are interested in the critical end point which denotes a critical point connecting two different types of transitions. It is one of the most important features of QCD phase diagram. However, whether there is a CEP in the phase diagram or not is still highly debated in the literature and it depends on the chosen physical environment [47]. Our model indicates that there is a CEP for a small α but no CEP exists for a large α.

More restrictions on α and the type of phase transition could be hinted at by the experiments of RHIC. Note that the above calculations about the QCD phase diagram are in the conditions of neutron stars. For the experiments of RHIC, the conditions are quite different. An important difference is that the ratio of electric charge over baryon is special and is approximately 0.4, i.e., $n_q = 0.4 n_B$. Second, the strangeness neutrality requires the density of strange quark (n_s) to be zero. Additionally, the experiments of RHIC are not in β equilibrium, but are connected with an ambiguous chemical potential condition. However, comparing with the special electric charge condition, such a chemical potential condition will have less influence on the QCD phase diagram. To compare with the RHIC

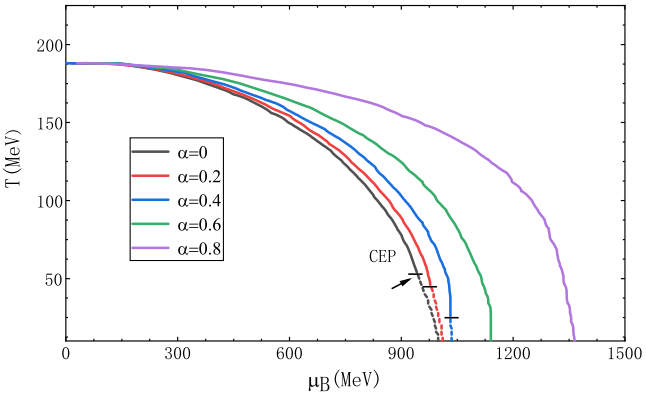

FIG. 3. The QCD phase diagram on the T-μ plane for different α for the conditions of neutron stars.

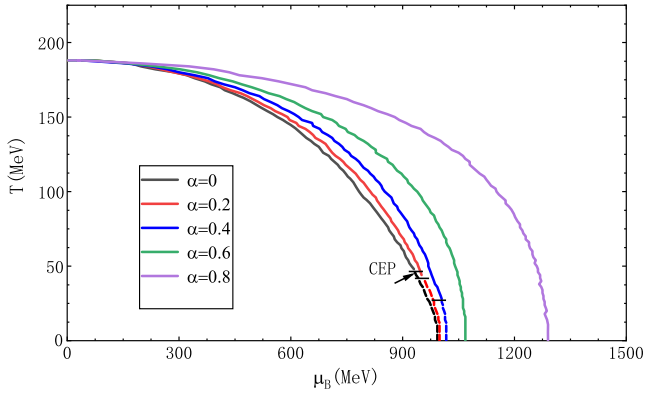

FIG. 4. The QCD phase diagram on the T-μ plane for different α, under the condition of $n_q = 0.4n_B$ and β equilibrium. When $\alpha > 0.58$, there is no CEP in our model.

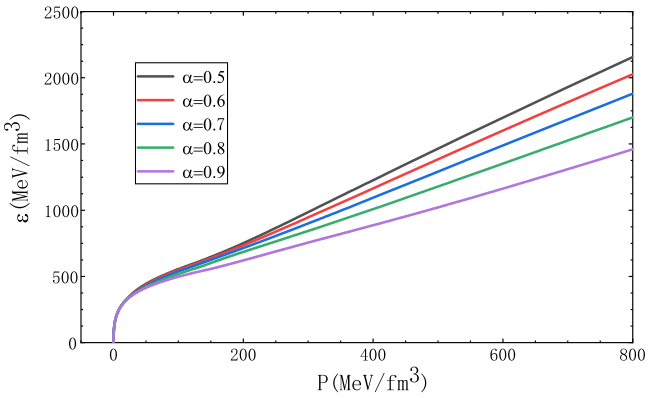

FIG. 5. The crossover equation of state for different α.

experiments, we have calculated the QCD phase diagram under the above experimental conditions (but still with β equilibrium). The results are shown in Fig. 4. In these cases, our model predicts that there will be no CEP when $\alpha > 0.58$ in the phase diagram.

III. HYBRID STARS WITH A CROSSOVER EQUATION OF STATE

The EOS plays a critical role in calculating the mass-radius relation and tidal deformability (Λ) of neutron stars. Using Eq. (10), we can get the quark section of the EOS. The hybrid star also includes a hadron section, but the NJL model makes it difficult to describe the hadron state at low densities. Thus we use the APR EOS for hadronic matter, which is a soft EOS [34]. It has been adopted by many authors to describe hybrid stars at low densities [48,49]. For the whole EOS, we use a simple mathematical method to link the hadron and quark section,

$$p = s(\mu)p_H(\mu) + (1 - s(\mu))p_Q(\mu), \tag{12}$$

$$n = \frac{dp}{d\mu} = s(\mu)n_H(\mu) + (1 - s(\mu))n_Q(\mu) + \frac{ds}{d\mu}(p_H - p_Q). \tag{13}$$

Here p_H and p_Q is the pressure of hadron and quark section, p is the total pressure. The case is similar for the density n. The function s is defined as

$$s(\mu) = e^{-\frac{\mu-\mu_0}{\mu_1}}. \tag{14}$$

Here the parameter $\mu_0 = 923$ MeV corresponds to the chemical potential that nucleon matter begins to appear in the ARP EOS model. The parameter $\mu_1 = 1200$ MeV we assume here can make the contribution of hadron matter reduce and the contribution of quark matter increase smoothly when the density changes from $2n_0$ to $8n_0$, which means it is a crossover between quark and hadron matter. So, a reasonable requirement is that the EOS of quark matter also has a crossover, which means $\alpha > 0.47$ here. The whole EOS is shown in Fig. 5, from which it can be seen that a larger α will lead to a harder EOS.

To study the stiffness of the system in detail, we calculate the square of sound velocity

$$v^2 = \frac{dp}{d\varepsilon}, \tag{15}$$

which can reflect the stiffness of the system. The results are plot in Fig. 6. From this figure, we can see that a larger α leads to a larger sound velocity, which demonstrates that the stiffness of the EOS will increase with α.

We then study the mass-radius relation by solving the Tolman-Oppenheimer-Volkoff equations (in the natural unit system)

$$\frac{dp(r)}{dr} = -\frac{(\varepsilon + p)(M + 4\pi r^3 p)}{r(r - 2M)}, \tag{16}$$

$$\frac{dM(r)}{dr} = 4\pi r^2 \varepsilon. \tag{17}$$

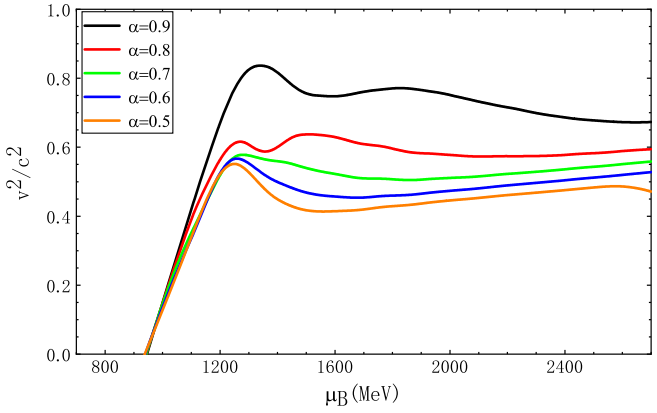

FIG. 6. The square of sound velocity for different α.

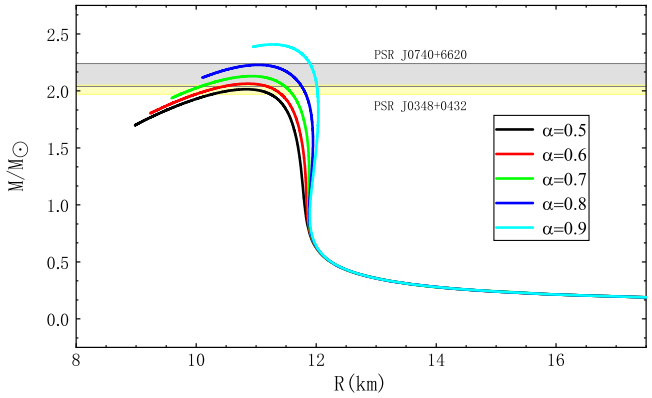

FIG. 7. Mass-radii relations of hybrid stars for different α. The maximum mass increases with α. Masses are in units of $M_\odot$.

In addition, we use the small-crust approximation [50] to describe the crust of our hybrid stars. To show the influence of α on the neutron star, the mass-radius relation of hybrid stars for different values of α is presented in Fig. 7. Astronomical observations show that the masses of pulsars (PSR): PSR J0384 + 0432 and PSR J1614-2230 are $2.01 \pm 0.04\ M_\odot$ and $1.928 \pm 0.017\ M_\odot$, respectively. Our result indicates that when $\alpha = 0.5$, the maximum strange matter star is $2.01\ M_\odot$, which is consistent with observations. However, when $\alpha = 0.5$ it is difficult to meet the requirement of PSR J0740 + 6620 ($2.14 \pm 0.10\ M_\odot$). Thus, we may need an even larger α, such as in the range of 0.6–0.8. As shown in Fig. 7, the maximum mass of hybrid stars increases with the parameter α. If a larger mass of neutron star is observed then a larger α will be preferred.

Another astronomical phenomenon that can be engaged to limit the range of α is the cooling rate of neutron stars. The direct Urca process provides the fastest neutrino emission in nucleon matter and quark matter. It is the main cooling mechanism in neutron stars [51]. The neutrino emission rate is density dependent; a high density will lead to a high emission rate, which makes the cooling of neutron stars faster. This could give us more restrictions on the EOS. We plot in Fig. 8 the density distribution inside

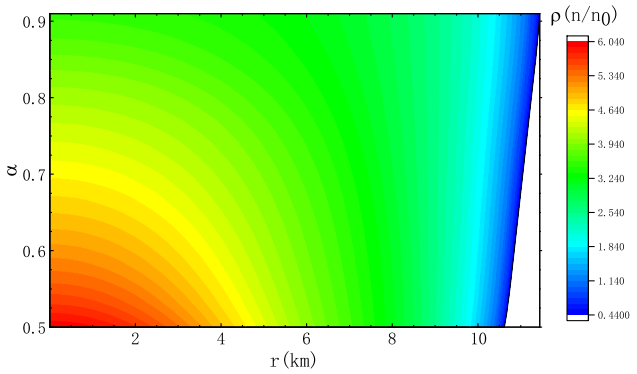

FIG. 8. The density distribution in a $2\ M_\odot$ hybrid star. The color depth denotes the density value.

a two solar mass hybrid star. We can see that a small α results in a high density, which will lead to a quicker cooling rate. A more detailed comparison is beyond the scope of this study and will be studied later.

During the inspiral and merger of two stars, the ratio of each star's induced-mass quadrupole moment to the tidal field is defined as the tidal deformability (Λ), and the Love number k_2 describes the distortion of the surface of a star. The relation between the tidal deformability (Λ) and the $l = 2$ dimensionless tidal Love number k_2 is (in the natural unit system)

$$k_2 = \frac{3}{2}\Lambda\left(\frac{M}{R}\right)^5. \tag{18}$$

According to Ref. [52], k_2 can be calculated as

$$\begin{aligned} k_2 = {} & \frac{8C^5}{5}(1-2C^2)[2+2C(y-1)-y] \\ & \times \{2C[6-3y+3C(5y-8)] \\ & + 4C^3[13-11y+C(3y-2)+2C^2(1+y)] \\ & + 3(1-2C)^2[2-y+2C(y-1)]\ln(1-2C)\}^{-1}, \end{aligned} \tag{19}$$

where $C = M/R$ is the compactness of the star, and

$$y = \frac{R\beta(R)}{H(R)} - \frac{4\pi R^3\varepsilon_0}{M} \tag{20}$$

is related to the metric variable H and surface energy density ε_0. The metric variable H depends on the EOS and can be obtained by integrating two differential equations

$$\frac{dH(r)}{dr} = \beta, \tag{21}$$

$$\begin{aligned} \frac{d\beta(r)}{dr} = {} & 2\left(1-2\frac{M}{r}\right)^{-1} H\left\{-2\pi[5\varepsilon+9p+f(\varepsilon+p)]\right. \\ & \left. + \frac{3}{r^2} + 2\left(1-2\frac{M}{r}\right)^{-1}\left(\frac{M}{r^2}+4\pi r p\right)^2\right\} \\ & + \frac{2\beta}{r}\left(1-2\frac{M}{r}\right)^{-1}\left[-1+\frac{M}{r}+2\pi r^2(\varepsilon-p)\right], \end{aligned} \tag{22}$$

where f is defined as

$$f = \frac{d\varepsilon}{dp}. \tag{23}$$

We can integrate Eqs. (22) and (23) from the center via expansions $H(r) = a_0 r^2$ and $\beta(r) = 2a_0 r$ for $r \ll R$ with

TABLE II. Properties of hybrid stars in our framework.

α	$M_{\max}(M_\odot)$	R(km)	$R_{1.4}(km)$	$\Lambda(1.4\ M_\odot)$
0.5	2.01	10.81	11.72	312
0.6	2.06	10.84	11.80	332
0.7	2.17	10.92	11.87	348
0.8	2.22	11.03	11.93	363
0.9	2.40	11.28	11.98	377

constant a_0. Since a_0 can be reduced in the expression of the Love number k_2, here we take $a_0 = 1$.

We have calculated the main parameters of hybrid stars for different α. The results are shown in Table II. For a 1.4 $M_\odot$ low-spin star, the tidal deformability (Λ) has been constrained in a range of (200, 800) through gravitational wave observations [53]. It can be seen that the results of our hybrid stars are consistent with the observational requirement.

IV. SUMMARY AND DISCUSSION

In this paper, we adopt a self-consistent mean field approximation to discuss the three-flavor NJL model. A free parameter α is introduced to denote the weight of different interaction channels. Using this method, we study the phase transition properties by calculating the chiral susceptibility. It is found that the (pseudo) critical chemical potential increases with α. We plot the QCD phase diagram under the condition applicable for neutron stars as well as the condition for heavy-ion collision experiments. It is found that there is no CEP when $\alpha > 0.47$ for neutron stars but for the heavy-ion collision experiments there will be no CEP when $\alpha > 0.58$. We discuss how the stiffness of EOS changes with α by examining the sound velocity. It is found that the phase transition of quark matter to hadron matter is a crossover when $\alpha > 0.47$ in neutron stars, thus we need a crossover connection method to describe the hybrid star. The corresponding EOS can also support a more massive star since it gets harder with a larger α. The density-radius diagram of a 2 $M_\odot$ hybrid star is plot to show the effects of different parameters. Finally we calculate the tidal deformability and show that our EOS can meet the requirements of gravitational wave observations.

To be specific, the EOS with $\alpha = 0.5$ yields a maximum compact star of 2.01 $M_\odot$, which can match the masses of PSR J1614-22300 ($1.928 \pm 0.017\ M_\odot$) [54] and PSR J0348 + 0432 ($2.01 \pm 0.04\ M_\odot$) [55]. However, $\alpha = 0.5$ is difficult to satisfy PSR J0740 + 6620 ($2.14 \pm 0.10\ M_\odot$) [56] and PSR J2215 + 5135 ($2.27^{+0.17}_{-0.15}$ [57]. A quark model with a larger α may provide a harder EOS to support a compact star with a larger mass. A more mild phase transition which means a larger α in this paper, makes quarks have a larger energy at the same density due to interactions with each other. As a result, $\alpha > 0.7$ is preferred to satisfy PSR J0740 + 6620 ($2.14 \pm 0.10\ M_\odot$) in our framework. More astronomical observations will help to further constrain the value of α. We calculate the density-radius distribution because the density of the matter may affect the cooling rate of neutron stars. Measuring the temperature of neutron stars may also help to constrain α.

ACKNOWLEDGMENTS

We thank the anonymous referee for helpful comments and suggestions. This work is supported by the National Natural Science Foundation of China (Grants No. 11873030, No. 12041306, and No. U1938201), by National SKA Program of China No. 2020SKA0120300, by the National Key R&D Program of China (2021YFA0718500), and by the science research grants from the China Manned Space Project No. CMS-CSST-2021-B11.

[1] B. P. Abbott, R. Abbott, T. Abbott, F. Acernese, K. Ackley, C. Adams, T. Adams, P. Addesso, R. Adhikari, V. Adya *et al.*, Phys. Rev. Lett. **119**, 161101 (2017).
[2] T. Damour, M. Soffel, and C. Xu, Phys. Rev. D **45**, 1017 (1992).
[3] É. É. Flanagan and T. Hinderer, Phys. Rev. D **77**, 021502(R) (2008).
[4] T. Hinderer, Astrophys. J. **677**, 1216 (2008).
[5] G. V. Dunne, Heisenberg-Euler effective Lagrangians: Basics and extensions, in *From Fields to Strings: Circumnavigating Theoretical Physics. Ian Kogan Memorial Collection (3 Volume Set)*, edited by M. Shifman, A. Vainshtein, and J. Wheater (World Scientific, Singapore, 2004), pp. 445–522.
[6] E. Berger, Annu. Rev. Astron. Astrophys. **52**, 43 (2014).
[7] M. C. Miller *et al.*, Astrophys. J. Lett. **887**, L24 (2019).
[8] J. Geng, B. Li, and Y. Huang, Innovations **2**, 100152 (2021).
[9] S. Bethke, Prog. Part. Nucl. Phys. **58**, 351 (2007).
[10] U. Vogl and W. Weise, Prog. Part. Nucl. Phys. **27**, 195 (1991).
[11] S. Klevansky, Rev. Mod. Phys. **64**, 649 (1992).
[12] T. Hatsuda and T. Kunihiro, Phys. Rep. **247**, 221 (1994).
[13] W. Fan, X. Luo, and H.-S. Zong, Int. J. Mod. Phys. A **32**, 1750061 (2017).
[14] C.-M. Li, P.-L. Yin, and H.-S. Zong, Phys. Rev. D **99**, 076006 (2019).
[15] O. Philipsen, Prog. Part. Nucl. Phys. **70**, 55 (2013).
[16] Z. Fodor and S. D. Katz, arXiv:0908.3341.
[17] S. Gupta, K. Huebner, and O. Kaczmarek, Phys. Rev. D **77**, 034503 (2008).

[18] S. Borsanyi, Z. Fodor, C. Hoelbling, S. D. Katz, S. Krieg, and K. K. Szabo, Phys. Lett. B **730**, 99 (2014).
[19] M. Aggarwal, Z. Ahammed, A. Alakhverdyants, I. Alekseev, J. Alford, B. Anderson, D. Arkhipkin, G. Averichev, J. Balewski, L. Barnby *et al.*, Phys. Rev. Lett. **105**, 022302 (2010).
[20] L. Adamczyk, J. Adkins, G. Agakishiev, M. Aggarwal, Z. Ahammed, I. Alekseev, J. Alford, C. Anson, A. Aparin, D. Arkhipkin *et al.*, Phys. Rev. Lett. **112**, 032302 (2014).
[21] L. Adamczyk, J. Adams, J. K. Adkins, G. Agakishiev, M. Aggarwal, Z. Ahammed, N. Ajitanand, I. Alekseev, D. Anderson, R. Aoyama *et al.*, Phys. Lett. B **785**, 551 (2018).
[22] F. Wang, Y. Cao, and H. Zong, Chin. Phys. C **43**, 084102 (2019).
[23] G. Baym and S. Chin, Phys. Lett. **62B**, 241 (1976).
[24] G. Baym, T. Hatsuda, T. Kojo, P. D. Powell, Y. Song, and T. Takatsuka, Rep. Prog. Phys. **81**, 056902 (2018).
[25] C.-M. Li, Y. Yan, J.-J. Geng, Y.-F. Huang, and H.-S. Zong, Phys. Rev. D **98**, 083013 (2018).
[26] Z. Bai and Y.-X. Liu, AIP Conf. Proc. **2127**, 020030 (2019).
[27] A. Masayuki and Y. Koichi, Nucl. Phys. **A504**, 668 (1989).
[28] J. O. Andersen and M. Strickland, Phys. Rev. D **66**, 105001 (2002).
[29] M. Fortin, C. Providência, A. R. Raduta, F. Gulminelli, J. L. Zdunik, P. Haensel, and M. Bejger, Phys. Rev. C **94**, 035804 (2016).
[30] C.-M. Li, J.-L. Zhang, Y. Yan, Y.-F. Huang, and H.-S. Zong, Phys. Rev. D **97**, 103013 (2018).
[31] H. Chen, M. Baldo, G. F. Burgio, and H. J. Schulze, Phys. Rev. D **84**, 105023 (2011).
[32] K. Masuda, T. Hatsuda, and T. Takatsuka, Prog. Theor. Exp. Phys. **2013**, 073D01 (2013).
[33] J. I. Kapusta and T. Welle, Phys. Rev. C **104**, L012801 (2021).
[34] A. Akmal, V. R. Pandharipande, and D. G. Ravenhall, Phys. Rev. C **58**, 1804 (1998).
[35] T. Hatsuda and T. Kunihiro, Prog. Theor. Phys. **74**, 765 (1985).
[36] Y. Nambu and G. Jona-Lasinio, Phys. Rev. **122**, 345 (1961).
[37] T. Kunihiro and T. Hatsuda, Prog. Theor. Phys. **71**, 1332 (1984).
[38] M. Buballa, Phys. Rep. **407**, 205 (2005).
[39] L.-K. Yang, X. Luo, and H.-S. Zong, Phys. Rev. D **100**, 094012 (2019).
[40] L.-Q. Su, C. Shi, Y.-H. xia, and H. Zong, Phys. Rev. D **102**, 054028 (2020).
[41] T. Zhao, W. Zheng, F. Wang, C.-M. Li, Y. Yan, Y.-F. Huang, and H.-S. Zong, Phys. Rev. D **100**, 043018 (2019).
[42] R. C. Pereira, P. Costa, and C. Providência, Phys. Rev. D **94**, 094001 (2016).
[43] J. Kapusta and C. Gale, *Finite-Temperature Field Theory: Principles and Applications*, Cambridge Monographs on Mathematical Physics (Cambridge University Press, Cambridge, England, 2006).
[44] N. K. Glendenning, *Compact Stars: Nuclear Physics, Particle Physics and General Relativity* (Springer Science & Business Media, New York, 2012).
[45] Y. Aoki, Z. Fodor, S. Katz, and K. Szabó, Phys. Lett. B **643**, 46 (2006).
[46] K. Fukushima and T. Hatsuda, Rep. Prog. Phys. **74**, 014001 (2011).
[47] P. Costa, M. Ferreira, H. Hansen, D. P. Menezes, and C. Providência, Phys. Rev. D **89**, 056013 (2014).
[48] S. Y. Lau, P. T. Leung, and L. M. Lin, Phys. Rev. D **95**, 101302 (2017).
[49] M. Marczenko, D. Blaschke, K. Redlich, and C. Sasaki, Phys. Rev. D **98**, 103021 (2018).
[50] J. L. Zdunik, M. Fortin, and P. Haensel, Astron. Astrophys. **599**, A119 (2016).
[51] D. G. Yakovlev and C. J. Pethick, Annu. Rev. Astron. Astrophys. **42**, 169 (2004).
[52] T. Damour and A. Nagar, Phys. Rev. D **80**, 084035 (2009).
[53] A. Bauswein, N.-U. F. Bastian, D. Blaschke, K. Chatziioannou, J. A. Clark, T. Fischer, H.-T. Janka, O. Just, M. Oertel, and N. Stergioulas, AIP Conf. Proc. **2127**, 020013 (2019).
[54] E. Fonseca *et al.*, Astrophys. J. **832**, 167 (2016).
[55] J. Antoniadis *et al.*, Science **340**, 6131 (2013).
[56] H. T. Cromartie *et al.* (NANOGrav Collaboration), Nat. Astron. **4**, 72 (2020).
[57] M. Linares, T. Shahbaz, and J. Casares, Astrophys. J. **859**, 54 (2018).